Unintended consequences: Why carbonation can dominate in microscale hydration of calcium silicates

Nicola Ferralis,[a),c)] Deepak Jagannathan,[c)] Jeffrey C. Grossman, and Krystyn J. Van Vliet[b)]
Department of Materials Science and Engineering, Massachusetts Institute of Technology, Cambridge, Massachusetts 02139, USA

(Received 24 April 2015; accepted 15 July 2015)

This article is dedicated in honor of Dr. Hamlin Jennings, our esteemed colleague in cement chemistry who provided comment on this work and sadly passed just after its acceptance. His enthusiastic efforts to bring a materials science perspective to cement research will be long valued.

The initial microscale mechanisms and materials interfacial process responsible for hydration of calcium silicates are poorly understood even in model systems. The lack of a measured microscale chemical signature has confounded understanding of growth mechanisms and kinetics for microreaction volumes. Here, we use Raman and optical spectroscopies to quantify hydration and environmental carbonation of tricalcium silicates across length and time scales. We show via spatially resolved chemical analysis that carbonate formation during the initial byproduct in microscale reaction volumes is significant, even for subambient CO_2 levels. We propose that the competition between carbonation and hydration is enhanced strongly in microscale reaction volumes by increased surface-to-volume ratio relative to macroscale volumes, and by increased concentration of dissolved Ca^{2+} ions under poor hydration conditions that promote evaporation. This in situ analysis provides the first direct correlation between microscale interfacial hydration and carbonation environments and chemically defined reaction products in cementitious materials.

I. INTRODUCTION

The formation of the most ubiquitous engineered structural material concrete[1,2] is a complex reaction by which the cementitious binding phase is obtained by mixing calcium silicates with water.[3–5] As in all such complex hydrated composite materials that are nucleated in situ, it has remained challenging to validate which phases form (i.e., when and where). As a result, while several material processing steps are appreciated empirically, the dynamics of the interfacial hydration reaction mechanisms are understood poorly.[4,6] This limitation has confounded the development of new models and materials processes to manipulate the reaction kinetics and resulting properties of the phases,[1] as well as interpretation of laboratory-scale experiments that ostensibly monitor the formation of calcium-silicate-hydrates (often denoted C-S-H). In this particular class of hierarchical structural materials, the onset of hydration and C-S-H formation is thought key to overall reaction kinetics and subsequent mechanical durability of the hardened material. Furthermore, under realistic hydration conditions in presence of CO_2, reaction kinetics are further complicated by the formation of thermodynamically favorable carbonate by-products. Despite the crucial need to quantify mechanisms of early-stage hydrate formation at the microscale and its relation to carbonate formation, current understanding is based chiefly on observations in cement pastes at the macroscale. The underlying assumption is that the predominant chemical and hydration mechanisms are shared across these length scales.

At the macroscale, hydration of the calcium silicates to form C-S-H in the bulk is well known to overwhelmingly dominate the occurrence of surface carbonation. Indeed, the predominance of hydration by-products in early-stage reactions provides the mechanical integrity of the so-called cement paste. Current efforts to quantify the early-stage reaction by-products at the microscale (rather than macroscale) are based mainly on impressively detailed yet indirect observations, such as soluble ion concentration, heat release rate, morphology of reaction by-products or soft x-ray analysis of silicate suspensions.[7–11] These approaches enabled comparative analysis of model systems, for example of nucleated phase morphology, but obfuscate clear identification of scale-dependent and competing chemical reactions and by-products. In this work, we present direct observations of interfacial hydration and carbonation of calcium trisilicate at microreaction volumes, which are

Contributing Editor: Lennart Bergström
Address all correspondence to these authors.
[a)]e-mail: ferralis@mit.edu
[b)]e-mail: krystyn@mit.edu
[c)]These authors equally contributed to this work.
DOI: 10.1557/jmr.2015.224

essential to infer length scale-dependent hydration kinetics at the microscale in relation to macroscale observations. A typical example of a scale dependent phenomenon during bulk hydration is surface carbonation in calcium trisilicate pastes due to Fickian diffusion of atmospheric CO_2 through the paste (detailed descriptions of relevant carbonation reactions described in SI and elsewhere[12]). At the macroscale, classification of different carbonate phases (e.g., vaterite, calcite, amorphous carbonates) and intermediate by-products (e.g., portlandite) and mechanisms of carbonate formation has also been proposed for paste-level reaction volumes, often complemented by several characterization methods.[13–17] At smaller volumes including the microscale, however, the applicability of these bulk mechanisms may not hold, due in part to the high surface-to-volume ratio at the microscale that can exacerbate evaporation effects. The balance between carbonation and hydration is determined by the surface area-to-volume ratio, which can vary from that of microscale inorganic particles to macroscale composite structures of meter-scale thickness. This multiscale variation also includes a broad range of conditions that influence carbonation during and well after this early-stage curing,[12,18,19] with both immediate and long-term consequences to structural stability and aging of concrete[20] (Details in SI).

To our knowledge, no direct observations of the formation of hydration and carbonation by-products for microscale reaction volumes have yet been proposed for ambient CO_2 concentrations present in air (<0.038 vol%). This work shows such incidental multiscale competition can occur at early reaction stages and depends on both the reaction volume and concentration of dissolved Ca^{2+} ions. While the chief byproduct of such solid and liquid reactions is hydrates under macroscopic and ideal environmental conditions and field materials processes, the findings described below indicate that nano to mesoscale formation models under realistic environmental conditions and laboratory experiments should consider the effects of presence of natural carbonation as an equally relevant microscale interfacial process during initial stages of cement hydration.[2,6] More generally, this environmentally reactive, multiscale-composite material[6] demonstrates the challenge and opportunity of materials process engineering afforded by direct, in situ, and spatially resolved quantification of microscale reaction products' chemical composition.[5]

II. EXPERIMENTAL DETAILS: PICOLITER CONFINED HYDRATION DROPLETS

We used a novel experimental design to access both the morphology and chemical identity of reaction products at the microscale. (See SI for details.) We adapted an experimental design reported previously to study the nucleation of crystalline materials such as NaCl and macromolecules such as solvated proteins.[21] Through this approach, spatially and temporally controlled nucleation can be initiated by creating confined supersaturated solutions. This is achieved by creating an array of picoliter volumes of aqueous solution on a glass cover slip, covering the picoliter droplets with an organic liquid to encourage slow diffusion of water. The resulting array of supersaturated confined volumes allows the observation of nucleation and growth processes via an optical microscope. Time-lapse image acquisition (and related image analysis) and in situ Raman spectroscopy were conducted within microscale regions within individual droplets, as described below. The former was used to quantify the growth kinetics of reaction by-products, while the latter was used to characterize the chemical and mineral identity of the hydration and carbonation by-products.

III. RESULTS AND DISCUSSION

A. Morphological characterization of microscale reactions

To identify the chemical attributes of microscale reaction products formed when water is mixed with this model calcium silicate phase under ambient conditions, the monoclinic tricalcium silicate Ca_3SiO5 (C_3S), we conducted optical and microRaman spectroscopy (μRS) (see Methods in the SI) under two different conditions: high initial ratios of water-to-solid (w/s ~ 100) and lower ratios typical of infrastructural cement pastes [w/s ~ 0.5 (Ref. 22)]; see SI and Figs. S.1–S.4 for Methods. While calcium silicates used in cement clinkers can contain elemental impurities including Al and Fe, we chose C_3S (the predominant component) to minimize the range of chemically distinct reaction products. The findings from both microRaman and time-lapse optical studies were then compared to bulk macroscale cementitious systems in which the reaction interface between cement and water is not directly accessible. Hardened cement pastes with w/s ~ 0.5 were hydrated for durations ranging between several hours to 1 wk.

Morphological changes and growth regimes upon exposure of tricalcium silicate to water were monitored via time-lapse optical microscopy [Fig. 1, see also Fig. S.3(a)], using an experimental technique developed by Grossier et al.[21] to visualize crystal nucleation, as described in Experimental Details and in SI. Note that this optical analysis provides a basis of visual and quantitative comparison with others' morphological characterization but does not chemically identify the observed products. Here, we tracked evolution of product reaction in picoliter-scale droplets of supersaturated, degassed aqueous solutions containing tricalcium silicate

microparticles (details in SI). Reaction droplets were surrounded by paraffin oil to slow but not completely eliminate evaporation or gas exchange[22,23]; complete water evaporation occurred after 15 h. Image analysis of reaction product growth rates quantified interface motion away from the immersed particles [Fig. S.3(b); details in SI]. Figure 1(a) illustrates the growth of the hydration product interface, indicating projections extending radially such that growth fronts (red arrows) can be approximated by arcs. The measured growth rate of this interface, for C_3S particles within NaOH-containing droplets at pH 12, was ~0.5 μm/h. In every droplet exhibiting byproduct growth, once the reacting particles were covered with this distinct phase, we then observed a transition in the growth front at later times. The stable, radial progression then became "finger-like," dendritic projections of distinct optical contrast [Fig. 1(b) and Fig. S.8].

Particles exhibiting growth in Fig. 1 were covered within 6 h by the radially expanding reaction product; after this time, irregular projections initiated. This observation is consistent with a previous atomic force microscopy-based analysis of growth from lime-wetted tricalcium silicate pellet surfaces, in which Garrault et al. reported an initially flat precipitate (up to at least 4 h) that then transitioned to a less dense, porous topography; see Fig. S.5 and discussion.[8] Although those authors did not report the transition time, in the present experiments we found the initiation of the unstable growth front to vary among droplets, due ostensibly to particle geometry, interparticle spacing, and/or crystallographic orientation of the exposed facets. This morphological transition has been interpreted previously as a transition from interface-controlled to diffusion-driven kinetics.[8,18]

To further characterize the growth kinetics and possible controlling growth regimes, we measured the radial evolution of the expanding byproduct fronts as a function of time (as described in SI and Fig. S.6). Diffusion-limited, circularly spreading growth fronts are typically well described by power laws $R \propto t^{\alpha}$ ($\alpha \leq 0.5$), whereas interface-controlled reaction kinetics are linear with time t.[24,25] Our measured growth evolution was initially linear [Fig. 1(b), inset], highlighting the interface-controlled kinetics of the early stage reaction.[25] The differing transitions from linear regimes among regions also emphasize the competition between the growth mechanisms at the reaction front with the variable diffusion rate of reagents at the source (tricalcium silicate) particle (Fig. S.7). The subsequent irregular projections resulted from partial dissolution of the tricalcium silicate and water evaporation [Fig. 1(a), Figs. S.7 and S.8].

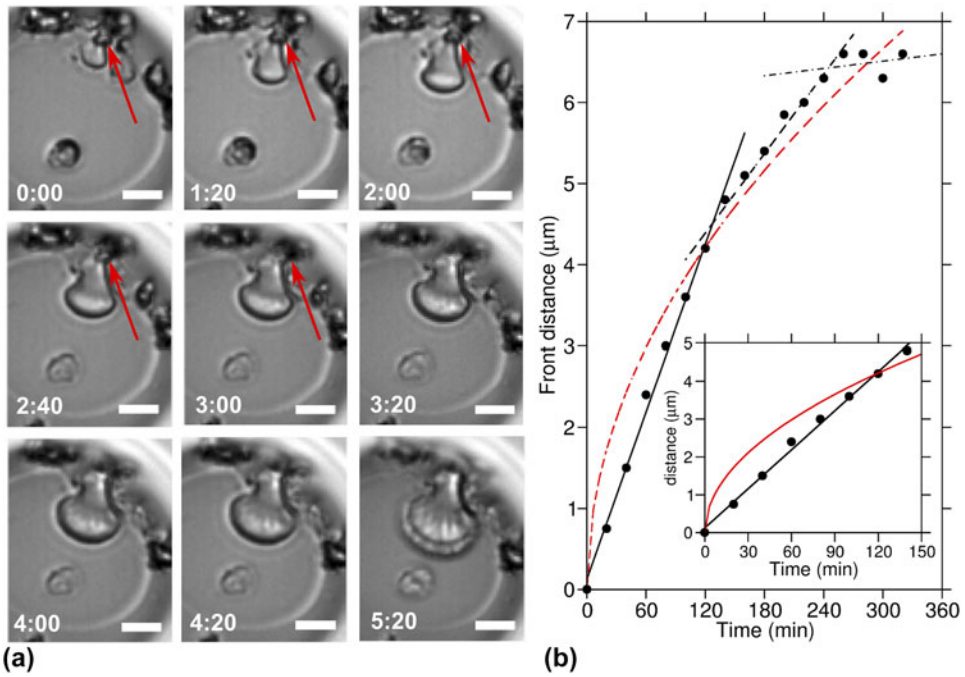

FIG. 1. Evolution of the product growth front inside an aqueous microdroplet. (a) Evolution of the reaction growth front of a reaction byproduct during hydration of tricalcium silicate, by optical microscopy (scale bar: 5 μm). Calcium trisilicate particles, indicated by the red arrow, contribute to the growth of the product. Initially (in this case, from 1–5:20 h), the growth front can be approximated as a smooth arc. Eventually (in this case, after 5 h), the growth front breaks up to develop rough "finger-like" projections. (b) The increment in the radius of the byproduct is measured directly from the optical images, as described in the SI. The growth evolution follows a series of linear regimes (black lines: linear fits). The overall growth profile does not follow a power law, $R \propto t^{\alpha}$ with $\alpha \leq 0.5$ (shown as a red curve in the inset), which is typical of a diffusion-limited growth regime.[22,23]

B. Chemical characterization of microscale reactions indicates predominant carbonation

Detailed interpretations of these growth mechanisms should not rely on an a priori assumption that C-S-H is the major reaction byproduct. We thus tested the validity of the assumption that C-S-H is the predominant reaction product within these microscale reaction volumes (which would support mechanisms proposed by Juenger et al.[10]; see SI) by explicitly identifying the chemical composition via μRS. RS is a critical approach for the characterization of chemical and mineral species in complex multiscale composites such as cementitious materials. In the context of industrial composites, RS is usually used at advanced stages of hydration for bulk cement pastes,[26–28] rather than the early stages of interest herein. (See SI for details and methods of RS experiments.) To our knowledge, this study is the first to leverage μRS to characterize the early stages of hydration and carbonation of calcium trisilicate for microscale reaction volumes. The key benefit of microRaman is comparable length scales of the probed volume and that of either the droplet (for microscale reaction volumes) or the near-surface region of a hydrating paste (for macroscale reaction volumes).

Figure 2 shows Raman spectra for tricalcium silicate particles hydrated for 2.5 h under the same conditions used to quantify morphological growth rates. The microscale interaction volume afforded spectral acquisition at several distinct locations. Based on the presence of very prominent peaks at 281 and 1085 cm^{-1} (corresponding to calcite) and the absence of any spectral signature corresponding to C-S-H, we identified the main product to be crystalline calcium carbonate ($CaCO_3$), rather than C-S-H (Fig. 2). It is expected that the Raman spectral sensitivity to calcium carbonates is approximately 30 times greater than that of C-S-H [defined by a broad spectral shoulder originating from Q1 silicates at 600–700 cm^{-1} (Ref. 26–28)], so the co-existence of both carbonate and hydrate phases cannot be excluded entirely from this observation alone. Alternatively, C-S-H formation can be assessed through reduction in peak intensity corresponding to the silicates on the anhydrous calcium trisilicate (~841 and 993 cm^{-1}), and the formation of other intermediary by-products (such as calcium hydroxide or portlandite). However, in the present experiments, no intensity reduction of the C_3S peak was observed, and a strong carbonate peak was present; this also supports the interpretation of these spectra as carbonate-dominated. We note that the observed calcium carbonate was found consistently and homogeneously throughout any point of the extending front that was observable via optical microscopy, and no by-products were detectable via microRaman signatures between the leading edges of the optically visible carbonate reaction fronts. Furthermore,

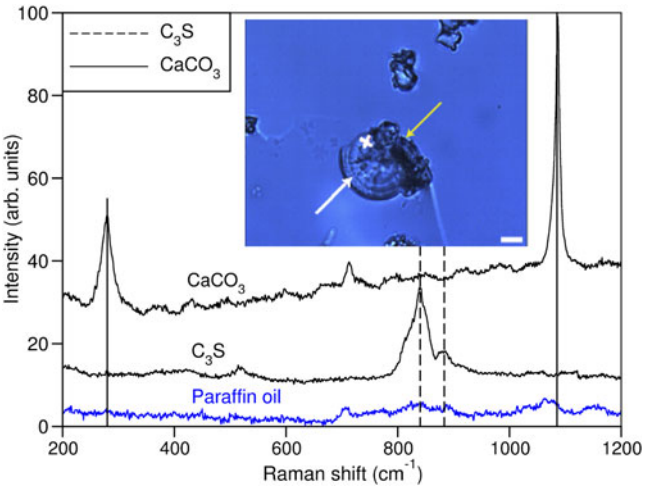

FIG. 2. Raman spectra of system comprising C_3S particles in NaOH pH 12 after 2.5 h of hydration. MicroRaman characterization of the chemical nature of the reaction by-products of hydration of tricalcium silicate C_3S, for which growth rates were computed from time-lapse image analysis. Raman spectra of pristine C_3S exhibited typical peaks at ~841 and 993 cm^{-1}. Raman spectra of the reaction byproduct of C_3S in NaOH pH 12 after 2.5 h of hydration were acquired at locations marked by a white cross in the inset optical image (scale bar: 5 μm). Spectral bands of the reaction by-products at 281 and 1085 cm^{-1} were consistent of those of calcium carbonate, which is formed by CO_2 diffusing through the paraffin oil. Inset: Optical micrograph showing the radially symmetric by-products (white arrows), extending from irregularly shaped C_3S microparticles (yellow arrows). These products share the same growth morphology as to those in Fig. 1(a).

within the time scale of early hydration prior to the acceleration period (2.5 h), significant formation of dense C-S-H by-products is not expected[5] and has not been observed previously.[29] Thus, despite the similar morphologies and growth rates of this product to previous reports of putative C-S-H,[10,23] we find that the early stage microscale product obtained in dilute, degassed aqueous suspensions under ambient conditions is not a hydration product but rather a carbonation product. We highlight that the observed calcium carbonate was formed within the hydrated volume, not ex situ upon exposure to higher ambient CO_2 concentrations, and the acquisition conditions of the Raman spectra were optimized to maintain the w/s ratio and minimally affect hydration (detailed in SI).

The rapid emergence of a stable crystalline form of calcium carbonate for microscale chemical reaction volumes (as probed with μRS in the pL droplet experiments as opposed to macroscale pastes) is in contrast with the formation of various surface carbonate phases in macroscopic pastes, from amorphous to vaterite and calcite.[15–17] This points to a rapid carbonate formation at the microscale, induced by a rapidly changing solvent composition within the microscale chemical reaction volume and enhanced by water evaporation, that is not common or expected within the calcium silicate hydration that proceeds in typical macroscopic bulk pastes.

C. Time and length scale-dependent susceptibility to carbonation

While not the chief product of calcium silicate hydration in typical bulk synthesis of cement pastes or concrete used for structural applications, the formation of surface carbonate by-products is usually artificially induced under CO_2 rich hydration conditions, rather than normal ambient conditions. Therefore, one may question the relevance of hydration and carbonation in microreaction volumes in relation to standard bulk processing conditions. We note that these experiments in pL-scale confined environments differ from typical bulk processing of cement pastes in two key characteristics: (i) water/solid ratio, w/s; and (ii) surface area-to-volume ratio, s/v (i.e., microscopic scale reaction volumes). Given that carbonation occurs through dissolved CO_2 in the aqueous media over several hours of observation, one would expect the high w/s ratio in the droplets to be the principal cause of carbonation, and that larger scale experiments at similarly high w/s ratios should also promote carbonation. However, this was not the case: Fig. 3(a) shows no evidence of calcium carbonate from the Raman spectra of a cement suspension with 10^8-fold greater mass of tricalcium silicate particles, as compared to pL-volume droplet experiments. Clearly, high w/s ratio is not the main driver toward extensive microscale carbonation.

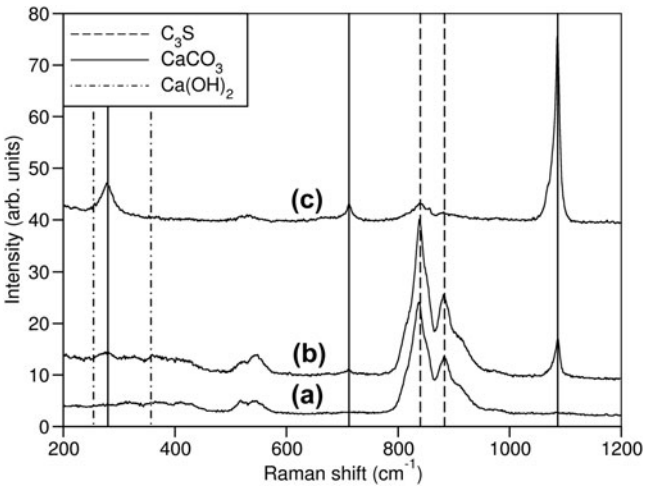

FIG. 3. Role of length scales of reaction volumes in carbonate formation at the early stages of tricalcium siliate (C_3S) hydration. (a) Raman spectra of a suspension of 500 mg of C_3S in 50 mL of water, with high water-to-solid ratio (w/s = 100) after 6 h of hydration: This paste had a 10^8-fold increase in tricalcium silicate mass as compared to picoliter-volume droplet experiments. The absence of the band at 1085 cm^{-1} indicates the absence of carbonates. (b) Raman spectra of the same amount of C_3S as in (a) after 6 h of hydration with uncontrolled evaporation of the aqueous media, but with a much lower water-to-solid ratio (w/s = 0.5) than that used in the picoliter-volume droplet experiment. Carbonation is clearly identified by the band at 1085 cm^{-1}. (c) The significantly higher intensity of the carbonate peak in the Raman spectra of the same hydrated C_3S in (b), but after laser-induced enhanced water evaporation, shows that enhanced evaporation strongly favor carbonate formation, even at larger reaction volumes.

It is known that carbonation is enhanced if the w/s ratio was reduced to approach levels typical of cement paste synthesis in excess of CO_2. Figure 3(b) shows that a cement paste of w/s ratio reduced to 0.5, mixed and then cured for 6 h in air with uncontrolled evaporation of aqueous media leads to formation of calcium carbonates. We infer that the change in surface area/volume ratio leads to a substantially different and dominating surface reaction dynamics, which cannot necessarily be assumed to remain the same as in bulk. Furthermore, the extreme sensitivity to carbonation for microscale reaction volumes, and the low levels of CO_2 needed (<0.038 vol%) to promote this, underscores the essential requirement of assessing in situ and in real time the dynamical evolution of the reaction product composition under realistic environmental conditions that include such species. Whenever such conditions cannot be satisfied (e.g., ex situ or in vacuo), only a static snapshot of the reaction conditions and by-products can be expected; such conditions can also modify the by-products via exposure to air and/or dehydration.

To further demonstrate the crucial role of water evaporation in the preferential formation of calcium carbonate, we artificially enhanced the formation of calcium carbonates by accelerating evaporation at ambient, constant (CO_2) via heating induced by the Raman excitation laser-probe at full power [Fig. 3(c), with details in SI]. We note that while a nonadiabatic environment within the micro reaction volume limits the quantification of heat transferred by the laser, optimization of the laser power levels between 1 and 50 mW/m^2 was sufficient to guarantee from none to rapid evaporation. Further, based on the kinetic analysis of growth mechanisms above, we posit that the mobile species within the aqueous media are the Ca^{2+} ions supplied from the C_3S particle. During interface-controlled growth, evaporation increases the local concentration of Ca^{2+} ions, due to both continued ion leaching from the tricalcium silicate particle and reduced water volume. Once a critical concentration of Ca^{2+} ions is reached at the microscale, cations are available for two competing reactions: hydration and/or carbonation. Our findings show that the thermodynamically preferred reaction is carbonation. Even assuming that hydration by-products could form under these conditions but that their spectral signature was to be below detection limits (due to the low Raman spectral sensitivity of C-S-H compared to carbonates), the very rapid reaction times (below 5 s) would not be favorable toward the much longer the formation time of C-S-H.[5,29] From these results, we conclude that susceptibility of cementitious systems to carbonation is modulated strongly by the evaporation rate of aqueous media—and therefore by

the locally high concentration of Ca^{2+} ions that can depend on reaction volume or calcium silicate volume—but not by the initial ratio of water to calcium silicates.

D. Mechanisms of carbonation, hydration acceleration, and suppression

Microscale understanding of the evolution of Ca^{2+} supersaturation induced by evaporation is essential in optimizing carbonate formation, whether enhancement or suppression is the goal. Such insight applies to both applications and mechanistic studies of interfacial growth of hydration products in cementitious materials. Furthermore, while it is typically desirable to promote hydration over carbonation in macroscale structures, in specific applications the capacity to control and therefore tune early stage carbonation at the microscale may facilitate certain hydrate/carbonate mixtures.[14] Thus, we investigated potential chemical approaches to control and reduce surface carbonation during early stage hydration induced by enhanced evaporation, benefiting from ability to probe microscale volumes with μRS. We note that such approaches to modulate carbonation can also be explored empirically, for example in enabling chemical reactions that prevent Ca^{2+} and CO^{2-} ions from reacting.[30] However, μRS can elucidate the reasons why such processing conditions work.

For evaporation-influenced carbonation, aqueous media is the source of both Ca^{2+} and CO^{2-} ions. Use of an acidic aqueous medium could suppress carbonation by effectively increasing the solubility limit of calcium carbonate[30] without solvating the Ca^{2+} ions required of hydration products, such as C-S-H and $Ca(OH)_2$. We explored this possibility by comparing early-stage cement pastes hydrated with neutral deionized water and acidic HCl (pH 2) solution. Note that this strategy is most effective within the first ~10 h of hydration when the paste is moist (i.e., damp but not immersed). Figure 4(a) compares Raman spectra of cement pastes of w/s = 0.5 using water or this acidic media and hydrated in a high relative humidity environment to minimize evaporation of aqueous media. Hydration spectra at 3 h showed early signs of carbonate formation for pastes initiated with water.

We note that the carbonate signature at ~1085 cm^{-1} (Ref. 26) is broad compared to standard crystalline calcite, suggesting the structure is not fully crystalline or includes other carbonate polytypes such as vaterite [Fig. S.9, Refs. 15–17]. The principal hydration product, low density C-S-H,[29] at very early stages of hydration may have a similar morphology as carbonation, underscoring the importance of chemical characterization of early stage reaction products. In contrast, pastes hydrated with acidic media exhibited a spectral band at ~1085 cm^{-1} of lower intensity after 3 h, indicating the presence of little or no carbonates; but spectra at later times up to 10 h in these samples showed comparatively sharper carbonation signatures. At these later time points, it is likely that acidity of the aqueous medium was not maintained sufficiently controllable to prevent the precipitation of calcium carbonate: continuous dissolution of tri-calcium silicate in the aqueous media increases the concentration of Ca^{2+} ions, eventually rendering acidity ineffective against carbonation. Thus, for aqueous media at initial pH 2, we find this critical time to be between 3 and 6 h.

Carbonation during early-stage hydration can also be suppressed, perhaps counter intuitively, via mechanical mixing that minimizes the exposure of given surface to air and thus to evaporation. These conditions have long been met empirically in macroscale processing, which typically includes copious addition of water at early stages and mechanical mixing of reacting suspensions. Figure 4(c) provides microscale analysis that elucidates one reason that this practice is beneficial: longer mixing times (30 min) reduced carbonate formation and promoted phase heterogeneity throughout the paste volume (probed through at least 20 μRS spectral scans), whereas brief mixing (5 min) in air promoted phase heterogeneity at only the paste surface. This observation supports the concept that mechanical mixing can overcome poor hydration conditions that would otherwise fail to homogenize the Ca^{2+} concentration throughout the macroscale volume itself and avoids imbalances due to longer exposures of a particular portion of the macroscale volume to air evaporation. Figure 4(d) summarizes this dependence of carbonation on CO_2 gradients such as those extending from an air-exposed surface of the reacting aqueous suspension.

E. Relating reaction mechanisms across time and length scales

These results for microscale reaction volumes, contrasted with macroscale volumes, shape the understanding of "surface" and "bulk" regions within macroscale, hydrating calcium silicate pastes. For a microscale particle, hydration conditions can deviate substantially from the expected "bulk" behavior, similarly to the surface of a macroscale sample. Hence, the microscale reaction volume can be considered a realistic representation of the paste surface, and more generally of microscale regions exposed to even ambient CO_2 concentrations. For example, the microscale reactions may favor carbonation at the bulk level at early-stage hydration of concrete with high degrees of air entrainment (i.e., many internal micropores, where the internal pore wall is exposed to the entrapped air during early-stage hydration).[31,32] In this way, it is not unexpected that the predominant reaction products differ as a function of length scale, as well as with time scale. For example, we did not observe significant spectral signature of hydration products such as $Ca(OH)_2$ and C-S-H in the Raman spectra of these

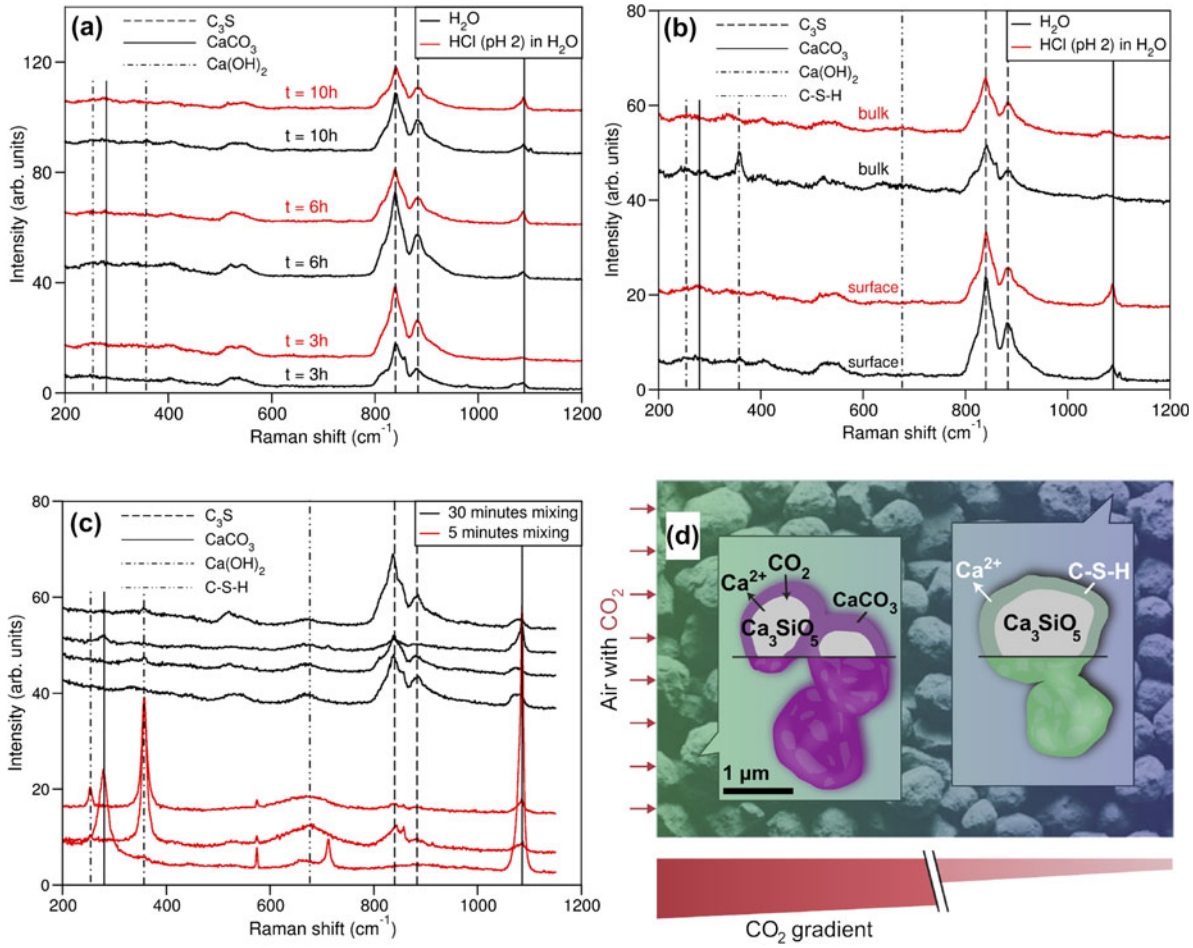

FIG. 4. Carbonation dynamics through hydration acceleration and suppression. (a) Calcium carbonate formation induced by water evaporation is mitigated through the use of acidic aqueous medium, as indicated by the low intensity of the calcium carbonate band in the Raman spectra on the surface of C_3S pastes mixed an aqueous solution of HCl pH 2 after 3, 6, and 10 h of hydration. (b) The crucial role played by evaporation in carbonate formation is evident in the absence of $CaCO_3$ Raman band in the bulk of C_3S pastes mixed with deionized water and HCl pH 2 after 10 h of hydration. The intensity of the $CaCO_3$ band is instead rather significant at the surface of the same paste. (c) Reduction in surface carbonation and increase in paste hydration homogeneity are also achieved by extending the initial mixing time (5 and 30 min, respectively, with hydration times up to 75 h). (d) Schematic of surface carbonation mechanisms induced by the gradient in CO_2 concentration from the environment into a suspension or paste. Scale bar is approximate in this schematic.

paste surfaces 10 h after initial mixing, for addition of either neutral or acidified (HCl, pH 2) water. (See SI and Fig. S.9 for discussion of longer time scales.) Referencing previous studies on pastes with similar hydration conditions (particle size ~ 50 μm and w/s ~ 0.5), this hydration time point lies toward the end and rate-maximum of the hydration kinetics acceleration period.[5,33] Given that the acceleration period is associated with the nucleation and growth of the C-S-H phase, the observed lack of C-S-H signature can be attributed directly to a retardation of C-S-H formation and to surface carbonation suppressing the formation of hydration products.

At the macroscale, preferential surface carbonation is appreciated in practice. Here, direct chemical analysis of microscale regions within such macroscale samples also facilitates comparison through the thickness of macroscale cementitious pastes (details in SI), to elucidate the role of initial mix chemistry in speed and extent of carbonation at the surface versus the interior. Figure 4(b) compares the Raman spectra for the surface and bulk, in pastes hydrated for 10 h upon mixing with pure H_2O or HCl, pH 2. In spectra from bulk paste mixed with H_2O, we observed a sharp peak at 350 cm^{-1} attributable to $Ca(OH)_2$, as well as two broad crests at 600–750 cm^{-1} attributable to presence of both $Ca(OH)_2$ and C-S-H. In contrast, spectra from the bulk paste mixed with HCl exhibited a single broad crest centered approximately at 680 cm^{-1}. While this feature can be attributed to contributions from both C-S-H and $Ca(OH)_2$, given the absence of a $Ca(OH)_2$ peak at 350 cm^{-1}, we assign this broad feature to the C-S-H phase. Additionally, we note

that the acidic medium can deter the precipitation of $Ca(OH)_2$. These results are consistent with the concept that the C-S-H phase nucleates and grows in the acceleration period.[34,35] In sharp contrast to the bulk spectra, hydration products were not prominent spectral features of the paste surface [Figs. 4(a) and 4(b)] and therefore were substantially delayed compared to the bulk. This illustrates that surface carbonate formation in early stages of hydration for macroscale reaction volumes delays the formation of hydration products, such as $Ca(OH)_2$ and C-S-H, and supports an evaporation-based model of carbonate formation [Fig. 4(d)] in pastes hydrated for less than one day. In short, the rapid evaporation leads to predominant and fast carbonation reactions that compete with and limit the hydration reaction over long time scales, in particular for microscale reaction volumes comprising Ca_3SiO_5 and H_2O. This predominant carbonation in microscale reaction volumes is attributed to the fact that even subambient levels of CO_2 act as an important reactant in concert with dissolved Ca^{2+} ions in such volumes. That predominance of carbonation within small reaction volumes is of note, particularly in design of experiments that aim to probe the hydration processes relevant to the dominant reaction product in macroscale volumes.

IV. CONCLUSIONS

In summary, direct chemical analysis of microscale reaction products formed when mixing tricalcium silicate with water purposefully carried out under ambient or low-CO_2 conditions demonstrates the potential for an interfacial competition between carbonation and hydration for microscale reaction volumes (with high surface to volume ratio); the predominant product depends strongly on length and time scales. μRS confirms that calcium carbonates can nucleate heterogeneously on microscale Ca_3SiO_5 particle surfaces, over shorter time scales and to a greater extent than competing hydration reactions, for low water/tricalcium silicate ratios promoted by evaporation. We attribute decreased hydration to the depletion of calcium ions due to carbonate formation at such low water/tricalcium silicate ratios during the initial, interface-controlled growth of calcium carbonates. This carbonation can be an inadvertent byproduct in microscale, fundamental studies of hydration reactions or particle–particle interactions, even in degassed aqueous environments. Thus, micro- to mesoscale studies or interfacial materials process that aim to quantify early-stage hydration products and growth interfaces should not assume the chemical composition of microscale growth interfaces a priori based on ex situ morphological analysis in vacuum or in low-oxygen environments. Rather, such studies must be designed to account for realistic hydration environments that include surface sensitive reactivity phenomena (such as carbonation) that are not predominant in bulk, macroscale pastes.

The chemical insight of competing carbonation versus hydration processes at the microscale also indicates new interfacial processes to retard carbonation in microscale reactions, for example via acidification of the hydrating fluid, even under poor hydration conditions that may promote evaporation at exposed surfaces. Similarly, this approach enables systematic consideration of varying calcium silicate-based structures, compositions and impurity levels (beyond the model tricalcium silicate analyzed herein) that may promote the rate and extent of hydration. Further, this microscale analysis suggests engineering of the internal porosity to promote carbonation at the pore wall surfaces. Such iterative approaches to maximize the extent of hydration in macroscale applications of these cementitious materials can be guided by this understanding of competitive microscale reactions, which will inform and speed optimization of currently empirical processing methods and of predictive models.

ACKNOWLEDGMENTS

The authors acknowledge financial support from the MIT Concrete Sustainability Hub, with sponsorship provided by the Portland Cement Association (PCA) and the Ready Mix Concrete (RMC) Research & Education Foundation, and the U.S. Department of Homeland Security, Science and Technology Directorate, Infrastructure Protection and Disaster Management Division, under the direction of the Engineer Research and Development Center (ERDC), U.S. Army Corps of Engineers. We appreciate R. Grossier's implementation of the microdroplet apparatus and discussion of initial dissolution observations, as well as S. Yip and the late H. Jennings for helpful discussion.

REFERENCES

1. K.J. Van Vliet, R. Pellenq, M. Buehler, J.C. Grossman, H. Jennings, F-J. Ulm, and S. Yip: Set in stone? A perspective on the concrete sustainability challenge. *MRS Bull.* **37**, 395–402 (2012).
2. I. Amato: Green cement: Concrete solutions. *Nature* **494**, 300–301 (2013).
3. A. Allen, J. Thomas, and H. Jennings: Composition and density of nanoscale calcium–silicate–hydrate in cement. *Nat. Mater.* **6**, 311–316 (2007).
4. E. Gartner, J. Young, D. Dadot, and I. Jawed: *Structure and Performance of Cement*, 2nd ed. (Spoon, London, UK, 2002); pp. 57–113.
5. J. Bullard, H. Jennings, R. Livingston, A. Nonat, G. Scherer, J. Schweitzer, K. Scrivener, and J. Thomas: Mechanisms of cement hydration. *Cem. Concr. Res.* **41**, 1208–1223 (2011).
6. S. Yip and M. Short: Multiscale materials modeling at the mesoscale. *Nat. Mater.* **12**, 774 (2013).
7. S. Gauffinet, E. Finot, E. Lesniewska, and A. Nonat: Direct observation of the growth of calcium silicate hydrate on alite

and silica surfaces by atomic force microscopy. *Comptes Rendus de l'Academie des Sciences Series IIA Earth and Planetary Science* **327**, 231–236 (1998).
8. S. Garrault, E. Finot, E. Lesniewska, and A. Nonat: Study of CSH growth on C_3S surface during its early hydration. *Mater. Struct.* **38**, 435–442 (2005).
9. E. Gartner, K. Kurtis, and P. Monteiro: Proposed mechanism of CSH growth tested by soft X-ray microscopy. *Cem. Concr. Res.* **30**, 817–822 (2000).
10. M. Juenger, P. Monteiro, E. Gartner, and G. Denbeaux: A soft X-ray microscope investigation into the effects of calcium chloride on tricalcium silicate hydration. *Cem. Concr. Res.* **35**, 19–25 (2005).
11. M. Juenger, P. Monteiro, and E. Gartner: In situ imaging of ground granulated blast furnace slag hydration. *J. Mater. Sci.* **41**, 7074–7081 (2006).
12. L. Haselbach: Potential for carbon dioxide absorption in concrete. *J. Environ. Eng.* **135**, 465–472 (2009).
13. J. Young, R. Berger, and J. Breese: Accelerated curing of compacted calcium silicate mortars on exposure to CO_2. *J. Am. Ceram. Soc.* **57**, 394–397 (1974).
14. V. Rostami, Y. Shao, A. Boyd, and Z. He: Microstructure of cement paste subject to early carbonation curing. *Cem. Concr. Res.* **42**, 186 (2012).
15. K. Garbev, P. Stemmermann, L. Black, C. Breen, J. Yarwood, and B. Gasharova: Structural features of C–S–H(I) and its carbonation in air–A Raman spectroscopic study. Part I: Fresh phases. *J. Am. Ceram. Soc.* **90**, 900 (2007).
16. L. Black, C. Breen, J. Yarwood, K. Garbev, P. Stemmermann, and B. Gasharova: Structural features of C–S–H(I) and its carbonation in air–A Raman spectroscopic study. Part II: Carbonated phases. *J. Am. Ceram. Soc.* **90**, 908–917 (2007).
17. E. Dubina, L. Korat, L. Black, J. Strupi-Suput, and J. Plank: Influence of water vapour and carbon dioxide on free lime during storage at 80 °C, studied by Raman spectroscopy. *Spectrochim. Acta, Part A* **111**, 299 (2013).
18. J. Severinghaus, W. Broecker, W. Dempster, T. MacCallum, and M. Wahlen: Oxygen loss in biosphere 2. *EOS Trans.: AGU* **75**, 33–40 (1994).
19. C. Pade and M. Guimaraes: The CO_2 uptake of concrete in 100 year perspective. *Cem. Concr. Res.* **37**, 1348–1356 (2007).
20. R. Andersson, K. Fridh, H. Stripple, and M. Haglund: Calculating CO_2 uptake for existing concrete structures during and after service life. *Environ. Sci. Technol.* **47**, 11625 (2013).
21. R. Grossier, Z. Hammadi, R. Morin, A. Magnaldo, and S. Vessler: Generating nanoliter to femtoliter microdroplets with ease. *Appl. Phys. Lett.* **98**, 091916 (2011).
22. International Code Council: International Building Code, (2012).
23. R. Grossier and K.J. Van Vliet: Visualizing hydration products. *Concrete Sustainability Hub Research Profile Letter*. (MIT, Cambridge, MA, 2012).
24. D. Reuter, G. Gerth, and J. Kirschner: *Surface Diffusion*, Vol. **360**. (Plenum Press, New York, NY, 1997); p. 489.
25. N. Ferralis, F. El Gabaly, A. Schmid, R. Maboudian, and C. Carraro: Real-time observation of reactive spreading of gold on silicon. *Phys. Rev. Lett.* **103**, 256102 (2009).
26. L. Black: Raman spectroscopy of cementitious materials. *Spectrosc. Prop. Inorg. Organomet. Compd.* **40**, 72–127 (2009).
27. S. Martınez-Ramırez and L. Fernandez-Carrasco: *Construction and Building: Design, Materials, and Techniques*, Chapter 10 (Nova Science Publishers, Hauppauge, NY, 2011).
28. S. Potgieter-Vermaak, J. Potgieter, and R. Van Grieken: The application of Raman spectrometry to investigate and characterize cement, Part I: A review. *Cem. Concr. Res.* **36**, 656–662 (2006).
29. E. Gallucci, P. Mathur, and K. Scrivener: Microstructural development of early age hydration shells around cement grains. *Cem. Concr. Res.* **40**, 4–13 (2010).
30. J. Morse and A. Luttge: Calcium carbonate formation and dissolution. *Chem. Rev.* **107**, 342–381 (2007).
31. U. Cebeci: Pore structure of air-entrained hardened cement paste. *Cem. Concr. Res.* **11**, 257 (1981).
32. G. Cultrone, E. Sebastian, and M. Ortega Huertas: Forced and natural carbonation of lime-based mortars with and without additives: Mineralogical and textural changes. *Cem. Concr. Res.* **35**, 2278 (2005).
33. R. Berliner, M. Popovici, K. Herwig, M. Berliner, H. Jennings, and J. Thomas: Quasielastic neutron scattering study of the effect of water-to-cement ratio on the hydration kinetics of tricalcium silicate. *Cem. Concr. Res.* **28**, 231–243 (1998).
34. J. Thomas, H. Jennings, and J. Chen: Influence of nucleation seeding on the hydration mechanisms of tricalcium silicate and cement. *J. Phys. Chem. C* **113**, 4327–4334 (2009).
35. J. Thomas, J. Biernacki, J. Bullard, S. Bishnoi, J. Dolado, G. Scherer, and A. Luttge: Modeling and simulation of cement hydration kinetics and microstructure development. *Cem. Concr. Res.* **41**, 1257–1278 (2011).

Supplementary Material

To view supplementary material for this article, please visit http://dx.doi.org/jmr.2015.224.

Unintended consequences: why carbonation can dominate in microscale hydration of calcium silicates

N. Ferralis[1,*], D. Jagannathan[1,*], J.C. Grossman[1], K.J. Van Vliet[1]

[1]*Department of Materials Science and Engineering, Massachusetts Institute of Technology, Cambridge, Massachusetts, 02139 USA*
** These authors equally contributed to this work.*

Supplementary Information

S.1 Picoliter confined hydration droplet

Figure S.1 shows the experimental setup used to create supersaturated confined volumes for the growth of hydration and carbonation of tricalcium silicate products. A key component of these experiments is the creation of picoliter droplets of aqueous fluids achieved using a microinjector (Femtojet, Eppendorf-Nethler-Hinz, GmbH Hamburg, Germany). These microinjectors are connected to microcapillaries (Femtotip, Eppendorf-Nethler-Hinz, GmbH Hamburg, Germany) that deliver picoliter droplets of fluid upon controlled application of pressure. Arrays of independent confined reaction environments are achieved using a joystick-controlled micromanipulator that enables lateral sample translation of the microcapillary. The reaction between cement clinker (specifically, tricalcium silicate) particles and aqueous fluids, both deposited on the glass slide, is observed through an inverted optical microscope (Olympus America Inc, Chelmsford MA, using a 20X objective). Optical micrographs are collected fusing a 5.5 megapixel CMOS camera (Andor Technology PLC, Belfast, Ireland), connected to a workstation for local image storage and systematic analysis.

Figure S.1 Experimental setup. Picoliter droplets of aqueous media are delivered using microcapillaries (a) regulated by microinjectors (b). Micromanipulator (c) controlled by joystick (d) enables 3D motion of the microcapillary. The hydration reaction as it unfolds on the glass slide (e) can be observed through the optical microscope (f). Camera attachment of the optical microscope enables storing and subsequent analysis of images on a local computer.

Droplet synthesis Confined reaction volumes with few, controllable, nucleation events were created at room temperature with the following protocol. A suspension of monoclinic tricalcium silicate, Ca_3SiO_5 (termed C_3S in cement chemistry notation, with 45 μm fineness; W. R. Grace & Company), was obtained by dissolving 10 g in 50 mL of isopropanol in a plastic centrifuge tube. Immediately before an experiment, the content in the tube were perturbed by manual shaking and allowed to settle until a section of translucent supernatant develops. The tube was agitated lightly enough that the supernatant became opaque, but not vigorously enough to disturb the C_3S residue at the bottom of the tube. As the particles resettled, transparent, translucent and opaque sections develop in the supernatant. Approximately $\sim$ 50 μl sample was drawn from the translucent section (red in Figure S.2) of the supernatant to deposit on the glass coverslip. When the isopropanol evaporates, an irregularly shaped deposit of microscopic tricalcium silicate particles remained on the glass slide. Empirically, we found that samples of suspension (that will be deposited on the

glass slide) drawn either from the fully transparent or opaque sections of the supernatant resulted in a distribution of clinker particles that is too sparse or too dense, respectively. In the latter case, clinker particles can agglomerate to form clusters (Figure S.2), defeating the purpose of these experiments to access the reaction interface between cement clinker particles and aqueous media. A 100 μL volume of inert paraffin oil was drawn into a pipette to cover this deposit of tricalcium silicate particles on the glass slide. We gently brought the microcapillary in contact with the surface of the glass slide beneath the droplet of oil. We then created sequences of picoliter droplets of aqueous media (degassed in vacuum of 29" Hg for ∼3 hours) with diameter ∼ 50μm (see Figure S.3a). We explored three alternatives for hydrating aqueous media: water, NaOH solution (pH 12), and saturated solution of $Ca(OH)_2$.

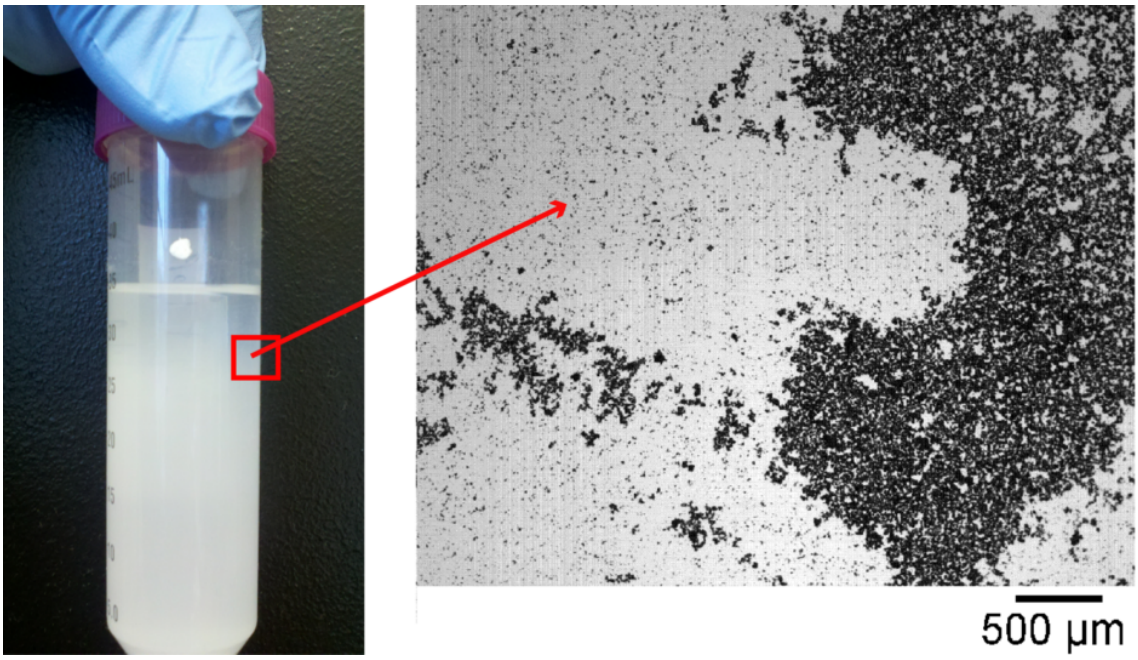

Figure S.2 (Left) Supernatant suspension of tricalcium silicate in isopropanol after agitation and decantation. The translucent supernatant is shown within the red square. (Right) Translucent supernatant (Approximately ∼ 50 μ) is deposited on a glass coverslip, with optimal dispersion.

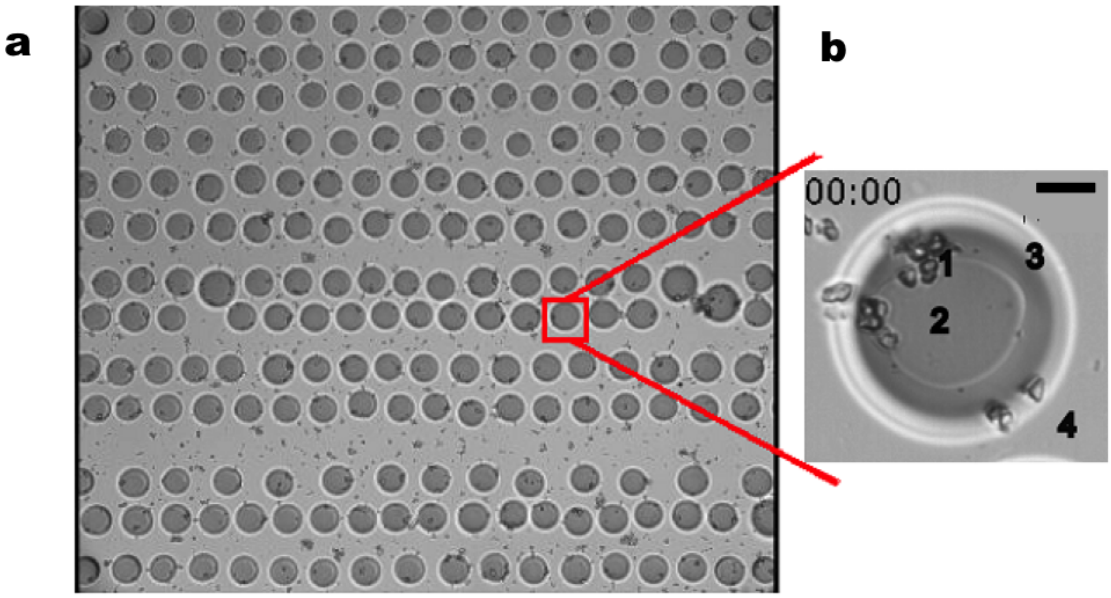

Figure S.3 (a) Array of picoliter droplets of NaOH pH 12 reacting with microscopic tricalcium silicate particles deposited on a glass slide observed under optical microscope. (b) Close-up view of one of the droplets at start of the experiment (time 00:00h, scale bar: 10 μm) with tricalcium silicate particles (1) at the periphery of the droplet of aqueous media (2). tricalcium silicate particles are also seen on the oil-water interface (3) and outside the droplet (4) in contact with oil. These particles do not undergo any reaction.

S.2 Reaction interface growth rates within droplets

The magnification provided by the optical microscope (objective: 20X) combined with the resolution of the CMOS camera, resulted in a spatial resolution of 0.3 μm/pixel. Reaction growth rates of the reaction interfaces within the droplet were measured using Cell Profiler ^{TM} [1] (Figure S.4a). We used the tracking module to compute the velocity (growth rate) of the reaction interface. The efficient use of tracking module required the tracked object (the reaction interface in this case) to be starkly distinct from the background. We achieved this contrast by subtracting the image at timestep $n-1$ from the image at timestep n, where a unit time step corresponds to 20 min. We found 20 min to be the smallest unit time step that produced detectable edges of the interface after the subtraction process. Time, t = 0, was chosen to denote the point in time when the reaction product became detectable at the scale of our observation ($\sim$ μm). The results of this process are shown in Figure S.4b. This process produced a sequence of images in which we can clearly contrast a white moving edge of the interface from the dark background. This sequence of images served as an input to the tracking module which then extracted the coordinates of the centroid of the moving edge as a function of time. Thus, time dependent growth rate was calculated as distance travelled between subsequent time steps (from coordinates of the centroid of the edge of the interface at times n and $n-1$) divided by unit time step (20 min). It is likely that the growing product adopted the symmetry of the space into which it is growing.

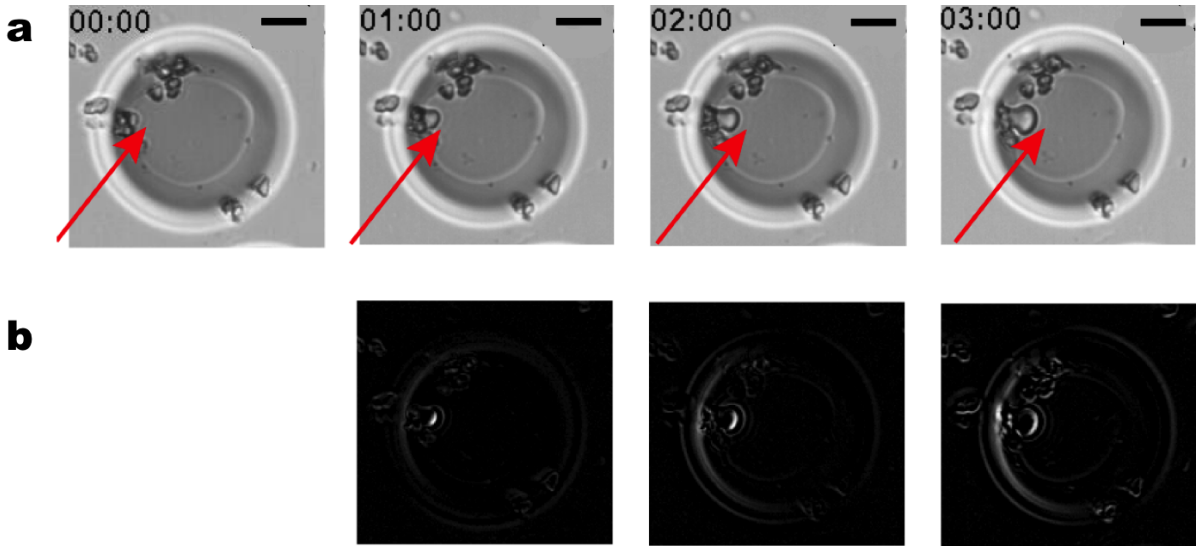

Figure S.4 (a) Dynamics of the reaction interface (red arrow points to leading edge of the interface) at 0, 1, 2, and 3 h. (b) Sequential image subtraction at time n from that at time $n-1$, $n \geq 1$ enabled high-contrast tracking of the interface and centroid that quantifies the rate of growth. (Scale bar: 10 μm)

We calculated growth rates of the interface that extended from reacting tricalcium silicate particles within these oil-confined picoliter aqueous droplets. The growth rates (Fig. S5) were calculated for tricalcium silicate particles reacting with droplets containing NaOH and at pH 12, and ranged from 0.05 to 1.5 μm/h with a mean +/- standard deviation of 0.77 +/- 0.25 μm/h. which are of the same order of magnitude as 0.1 um/hr calculated by [2] for wetting of a tricalcium silicate pellet imaged via atomic force microscopy [2]. Our measured growth rate of the initial, radially extending interfaces compares well with that calculated by Ref. [2] up until the morphology of the hydration product changed. To illustrate hydration product with "flat" morphology (and hence presumably constant growth rate), Ref. [2] included an AFM image taken at $t = 4$ h. Thus, we infer that the hydration product they observe exhibited a constant growth rate and flat interface for at least 4 h.

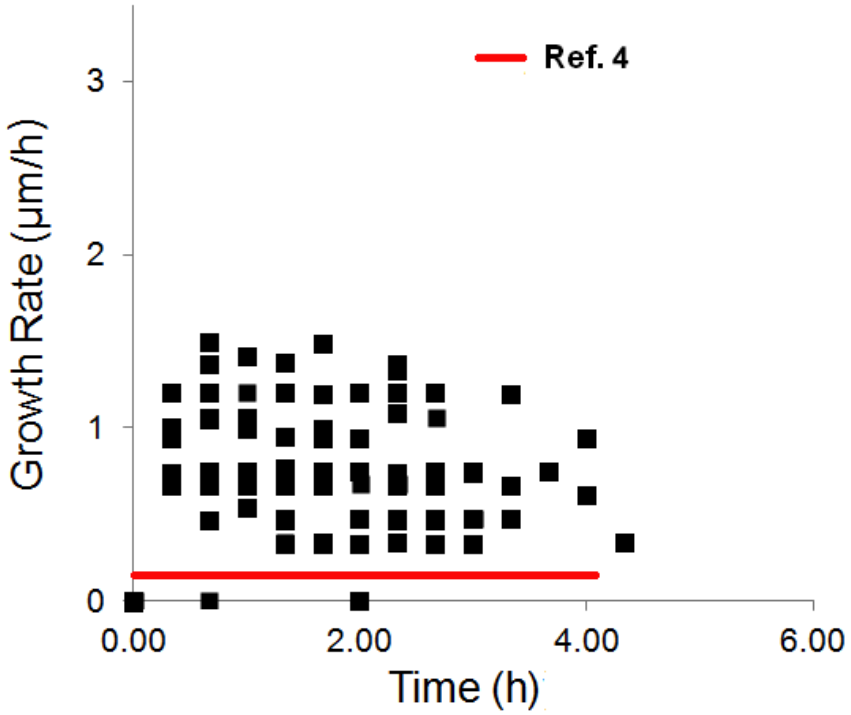

Figure S.5 Growth rates of hydration product computed by tracking growth fronts of 30 interfaces using image analysis algorithms described in the main text. Calcium trisilicate particles are reacting with aqueous droplets containing NaOH and at pH 12.

Our quantitative results on the growth rate of interface up until this growth front transition are consistent with lack of diffusion control in the initial stages of growth. Figure S.5 shows the results of our image analysis. We report growth rates of the interface up only within the interface-limited growth regime (and the growth front remains arc-like). We find average growth rates of $\sim$0.5 µm/h.

Effect of spatial distribution of calcium silicate particles on growth rates The differing spatial distribution of calcium silicate particles in each droplet did not have detectable effects on the growth rate of the product interface, within the instrumental resolution. It is important to note that the instrumental resolution is similar to the scale of the growth, and therefore the error could be of the same order of magnitude of the measured growth rates. In our limiting case, we can assert that the clinker particle distribution within/around the droplet influences the growth rate of the product interface within an order of magnitude. We note that our growth rates are the same order of magnitude as that reported in Ref. [2] for a flat growth front. We also note that the growth rates are relatively constant over the measured time periods. If the reaction were controlled by diffusion, the average growth rate at $t = 2$ h would be 4 times lesser than that at $t = 1$ h, that at $t = 3$ h would be 9 times lesser, and so on. Since we do not observe such a drastic decay of growth rates,

we further confirm that the growth kinetics is interfacially-driven.

The authors of that study do not confirm the chemical identity of the hydration product. However, they report that this hydration product grows by the aggregation of nanoparticles [2] (resolved using AFM to have dimensions of around 1000 nm^3).

S.3 Interfacial reaction growth kinetics

This surface nature of carbonation reactions (as opposed to the bulk nature of hydration reactions) is determined by the Fickian diffusion of CO_2 through from the paste surface into the bulk [3]. Therefore the diffusion-limited rate of carbonation is mainly responsible for the confinement of a carbonated surface layer, while minimal carbonation is expected and observed within the bulk. The rate of carbonation in macroscopic pastes can also be accelerated or artificially induced by increasing the CO_2 concentration, as well as by changing the Ca^{2+} supersaturation through different humidity conditions [4,5]. For quasi-two-dimensional (2D) systems, growth kinetics (and spreading) of mobile species from a reservoir over a flat surface are usually driven by diffusion, through wetting. Under the assumption that the spreading front from the nucleation site is circular or arc-like (with radius R), the atomic and molecular mobility on top of the surface is granted by the availability of such atoms/molecules from the reservoir. As the front grows, coverage is proportional to the area of the circular sector. Conceptually, as the front grows, the reservoir must be able to supply material to the front and the diffusion velocity from the reservoir to the front is the limiting factor. In pure 2D-diffusive systems, the front progression time t is proportional to R^2. For three-dimensional (3D) spherical growth, the front progression time t is proportional to the volume of the spherical sector, and therefore to R^3. For systems with more complex geometries (e.g., annular disks), the time dependence is $t \propto R^\beta$ ($\beta \geq 2$). For diffusion-limited systems, this dependence equates to $R \propto t^\alpha$ ($\alpha \leq 0.5$) [6,7]. For interface-limited systems, diffusion is such that the supply of mobile atoms to the growing front is constant, and therefore the concentration of mobile species at the reservoir and at the front is constant. The limiting factor is the series of processes, chemical reactions, and surface interactions that take place at the interface at the front [6,7]. The growth rate of the interface is therefore solely proportional to the extent of the interface itself, and therefore the growth time is proportional to the perimeter of the growth front (and so to its radius, R). The relation $R(t)$ is therefore linear.

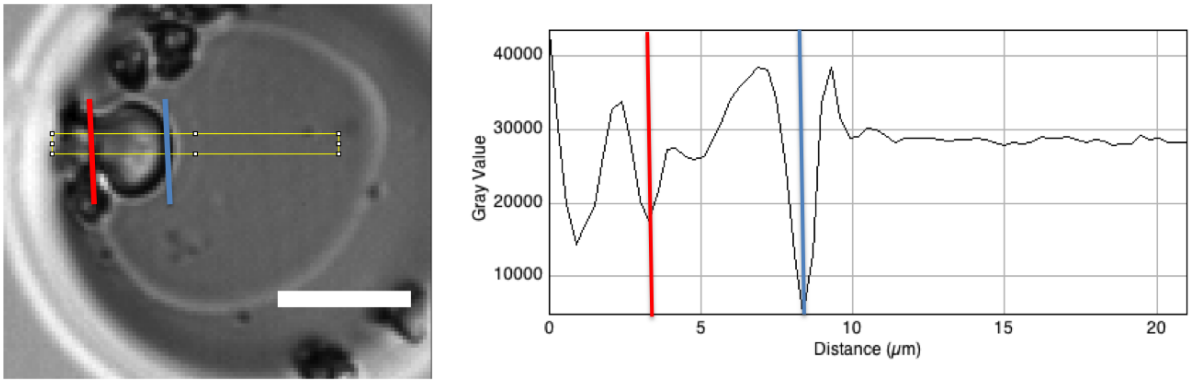

Figure S.6 Growth kinetics within a single droplet is measured from the optical images (scale bar: 10 μm), by integrated line profiles over the growing reaction product (as described in main text). The front edge of the reaction byproduct is highlighted in blue over the minimum of the profile. The tricalcium silicate particle is identified in the local minima highlighted by the red line.

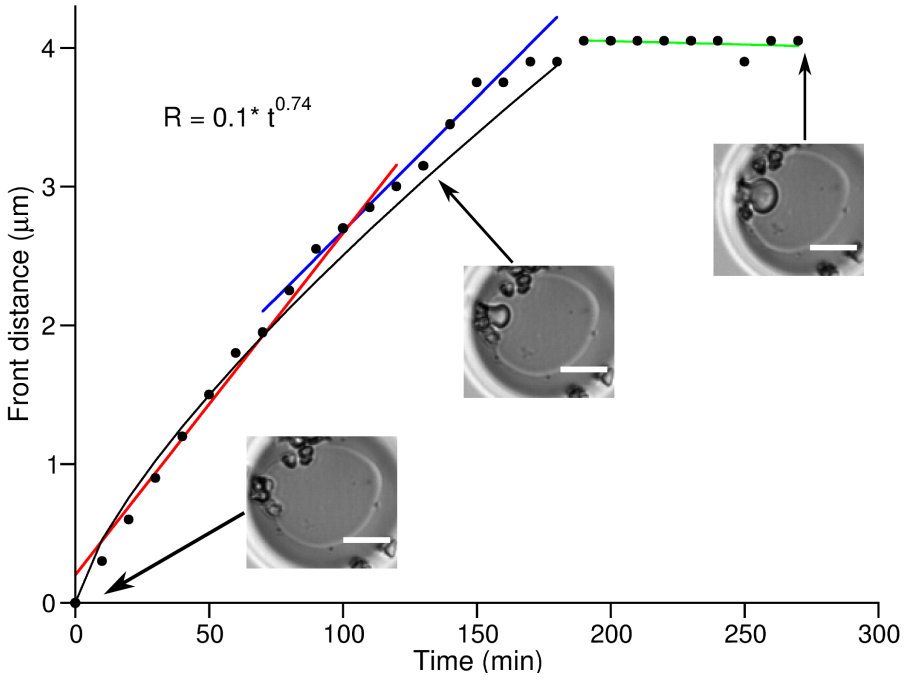

Figure S.7 Typical evolution kinetics of the growth profile measured from the C_3S particle. Growth and consolidation regimes are distinctively visible. Growth regimes follow power laws (black line) indicating an interface-driven growth mechanism, and within itself it can undergo different linear growth regimes (red and blue lines). During the consolidation regime, growth ends or it is significantly slower, indicating a diffusion-limited regime (green line). The images corresponding to the initial, intermediate and final growth stages are shown (scale bar: 10 μm).

Quantification of the growth kinetics in picoliter droplets Growth kinetics were analyzed by tracking the distance between the front of the growth product (carbonate, as confirmed by Raman spectroscopy) formation from the microparticle, through integrated line profiles (Figure S.6) via image processing software and analysis (ImageJ [8,9]). The image was oriented such that the growth direction of the reaction byproduct was horizontal. Therefore, the radius R of the arc-like front was measured by counting the number of pixels between the growing front and the C_3S particle, following a conversion through the image resolution. For each reactive particles analyzed, growth kinetics was extracted through a power-law fit ($R = A * t^B$), or by piecewise linear fits across different time ranges. Typical growth kinetics curves acquired from the C_3S particles in picoliter-volume droplets are depicted in Fig. 1b of the main text and Fig. S.7). The growth trend can be divided in two main regions: growth and consolidation. Growth regimes follow power laws with an exponent that is α >0.5 for every particle analyzed. This indicates that the growth kinetics is dominated by interface-driven growth mechanisms, as previously noted. (However, previous work has without proof attributed this growth reaction chemistry to hydration [2], rather than carbonation as shown in this work.) The mobile species are Ca^{2+} ions dissolved from the C_3S particle. This particle acts as a reservoir of Ca^{2+} ions, and the cation diffusion to the front is responsible for both nucleation at and subsequent growth of the carbonate away from the C_3S particle surface. While a reaction completely driven by interfacial processes would follow a linear trend, a very slow change in diffusivity of Ca^{2+} ions during the growth regime is responsible for an evolution that follows a power law with an exponent α between 0.7 and 0.9, rather than a linear trend. Furthermore, subregions of linear growth (red and blue linear fits in Figure S.7) can be observed, and the change in growth rate is directly attributed to the change in diffusivity. The small change in diffusivity of Ca^{2+} may be due to partial dissolution of the initial C_3S particle.

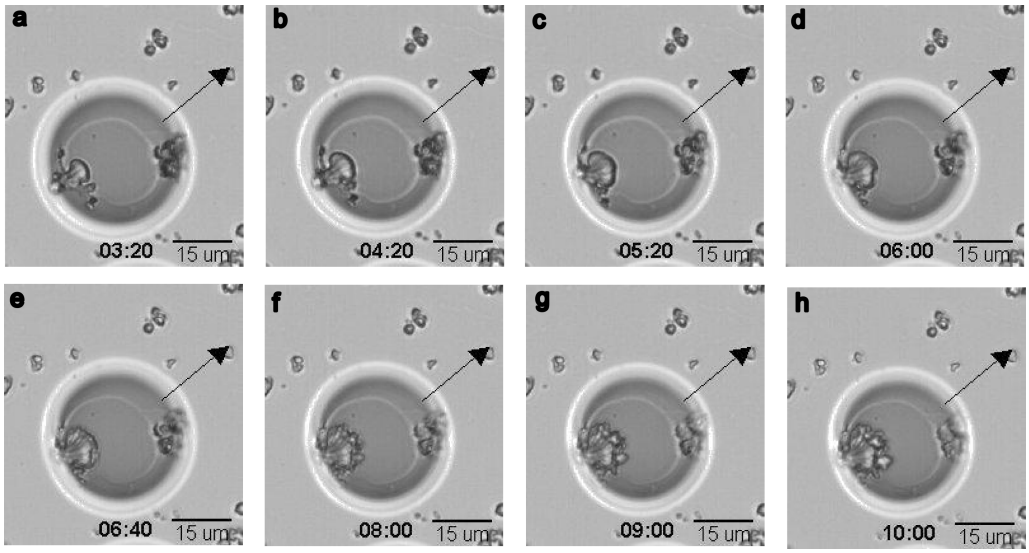

Figure S.8 Morphological evolution of the growth of reaction byproducts. The transition from Interface-limited growth (a-c) to diffusion limited growth (d-h) leads to the formation of dendrites. The arrow indicates the direction of growth, and time is indicated in hours:min.

A transition from interface-limited to diffusion-limited growth is observed when the growth ends or is severely retarded (green line in Figure S.7). The combination of C_3S depletion and water evaporation may ultimately reduce the available diffusive Ca^{2+} ions. Under this regime, the growth – if persistent – continues in a morphologically distorted growth front, typically through the formation of dendrites (Figure S.8) enabled by dissolved Ca^{2+} ions from the adjacent solution.

S.4 Mechanisms of accelerated C-S-H nucleation in C_3S via $CaCl_2$

$CaCl_2$ is a known reaction accelerator at the micro- to macroscales [10,11], but the mechanism by which this species enables a faster hydration rate has not been proven conclusively [10]. Based on x-ray microscopy studies of C_3S suspensions in $CaCl_2$ solution, Juenger *et al.* proposed that C-S-H was the reaction product formed in the early stages of hydration around the C_3S particle, and was more porous than that formed in conditions lacking $CaCl_2$; they posited that increased porosity enabled faster diffusion of water and calcium and silicate ions and, thus, higher growth rates of C-S-H [10]. On the other hand, Thomas *et al.*, based on modeling of experimental data from calorimetric experiments, proposed that $CaCl_2$ would influence the nucleation of C-S-H but would not affect the growth rate of C-S-H [12].

S.5 Cement paste preparation

Cement pastes were prepared at room temperature according to the following protocol. Five g of monoclinic tricalcium silicate (C_3S) were added to a glass vial with 2.5 g of aqueous media (water/solid ratio of 0.5) and mixed the contents using a stirrer for 5 mins. Approximately 0.5 g of the wet paste was transferred onto a glass slide using a spatula. Samples in which evaporation of aqueous media was not controlled were allowed to hydrate while exposed to ambient atmosphere. Other samples were sealed in a petri dish partially filled with deionized water so as to create an atmosphere of high relative humidity. Inside the Petri dishes, glass slides were secured on an elevated platform so as to avoid direct contact with a surrounding pool of water. This design does not fully prevent evaporation of aqueous media. Therefore, we further characterized areas of cement paste least susceptible to evaporation, i.e. the surface of the cement paste in contact with the glass slide. We label this surface as the "bulk" of the cement paste in the main text. After preparation, samples were exposed to the normal atmosphere only during the Raman spectroscopy experiments and were discarded afterwards.

S.6 Carbonation reactions during calcium trisilicate hydration

In absence of carbon dioxide, calcium trisilicate hydration is based on the reaction [11]:

$$C_3S + 3H_2O \rightarrow 3Ca^{2+} + H_2SiO_4^{2-} + 4OH^-$$

In presence of atmospheric carbon dioxide, this is dissolved in water to form carbonic acid [13]:

$$CO_2(g) + H_2O = H_2CO_3^*$$

$$H_2CO_3^* = H_2CO_3$$

Dissociation of carbonic acid leads to the formation of bicarbonate and carbonate ions:

$$H_2CO_3 = H^+ + HCO_3^{-1}$$

$$HCO_3^{-1} = H^+ + CO_3^{-2}$$

Formation of solid calcium carbonates results from the reaction of free Ca^{2+} ions (from the dissolution of calcium trisilicate and calcium hydroxide [13]) and CO_3^{-2} carbonate ions:

$$Ca^{2+} + CO_3^{-2} = CaCO_3(s)$$

S.7 Effects of hydration time scales on "surface" carbonation

As the time-scale of carbonation (and its effects on hydration) depends strongly on the length scale, it is important to reconcile surface phenomena with the expected and observed later stages of bulk hydration. At later stages of hydration ($\sim$1 day to 1 week), the presence of carbonates in cement pastes was seen as less pronounced. Figure S.9 shows Raman spectra for pastes maintained at high relative humidity atmospheres, minimizing evaporation of aqueous media while not changing exposure to CO_2 in the air. These spectra exhibited carbonate peaks at 2–4 days hydration that were reduced relative to those in Figs. 3 and 4a-b; significant levels of carbonation were observed only after 14 days. Under these conditions, the aqueous medium is consumed in the formation of $Ca(OH)_2$ and C-S-H, such that carbonation then takes place through reaction of these products directly with CO_2 in the atmosphere. For a given surface area of such porous reacting materials, moist pastes (hydrated one day or less) would then form calcium carbonates at the surface faster than pastes hydrated for a few days or more. This rate difference is attributable to the relative competition between water evaporation (resulting in carbonation for short hydration times) and carbonation (directly via the gaseous atmospheric CO_2 at long hydration times), as depicted in Fig. 4d.

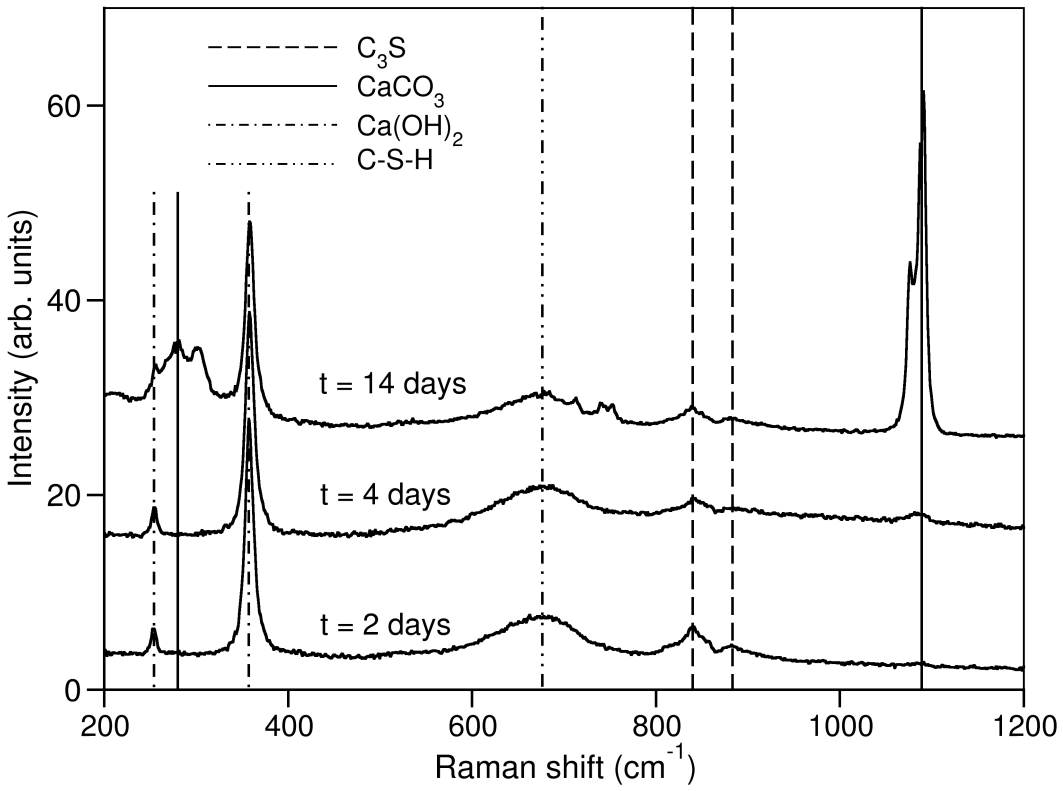

Figure S.9 Preservation of the water-to-solid ratio of 0.5 over longer periods of times (2 to 4 days) prevents the formation of calcium carbonate (highlighted by the absence of the $CaCO_3$ Raman band), and favors the formation of the expected hydration products, $Ca(OH)_2$ and C-S-H (characterized by the bands at 255 and 360 cm^{-1} for the former, and by the broad shoulder at 674 cm^{-1} for the latter [14]). The significant carbonate formation after 14 days coexists with the presence of the hydration products, $Ca(OH)_2$ and C-S-H, suggesting that the origin of $CaCO_3$ at later hydration stages, is not the result of evaporation, but rather by reaction of the hydration products with CO_2 [5].

S.8 Raman spectroscopy

Micro-Raman spectra were acquired (JY Horiba LabRam HR800 spectrometer in backscattering configuration), with an excitation line provided by a HeNe laser (excitation wavelength: 632.8 nm) through a confocal microscope (Olympus BX41, 100X objective). A 600 spectral grating was used, providing a spectral resolution of $\sim$1.2 cm^{-1}. Sample manipulation was carried out with a micro-mechanical stage to obtain high-lateral control over the position of the laser spot (diameter $\sim$ 800 nm for the excitation wavelength used, 632 nm). For each point of interest, five Raman spectra were acquired (with acquisition of five seconds each) and averaged. Because of the absence of fluorescence or any background, the analysis did not require special background subtraction.

In a typical experiment, picoliter droplets were grown on cover slips over glass slides. These slides were then transferred within few minutes from the synthesis under the optical microscope in the Raman spectrometer. Several droplets were selected and their location tracked (with accuracy of 100 nm), so the evolution of the same droplet could be at predetermined time steps. Raman spectroscopy measurements on hydrated pastes (prepared as described in Section S.5) were acquired on pastes transferred from the environmentally controlled environment to a glass slide. In light of the crucial role played by evaporation in the formation of carbonate species, both the surface of the cement paste (which is more susceptible to evaporation than its bulk) and the bulk itself were used for the measurement.

To minimize the contribution of evaporation induced by the excitation laser, a filter was used to reduce the power density to the sample to about 5 $\mu W/\mu m^2$. To ensure these acquisition parameters would induce no evaporation, several acquisitions were carried out in the same location with known hydration conditions. No detectable difference among the spectra were observed. For the experiments where laser-induced heating and evaporation was sought to accelerate carbonation, no filter was used and the maximum power density to the sample was approximately 50 $\mu W/\mu m^2$. Under these conditions, we observed a rapid formation of calcium carbonate, almost in real time (within the shortest time acquisition for individual spectra, 1 s).

Attribution of vibrational modes in the Raman spectra of pure and hydrated tricalcium silicate as well as calcium carbonates and calcium hydroxide were obtained from well-established literature [14–19].

References

1. Lamprecht, M., Sabatini, D., Carpenter, A. *et al.* Cellprofiler: free, versatile software for automated biological image analysis. *Biotechniques* **42**, 71 (2007).

2. Garrault, S., Finot, E., Lesniewska, E. & Nonat, A. Study of CSH growth on C_3S surface during its early hydration. *Materials and structures* **38**, 435–442 (2005).

3. Severinghaus, J., Broecker, W., Dempster, W., MacCallum, T. & Wahlen, M. Oxygen loss in biosphere 2. *EOS Transaction - AGU* **75**, 33–40 (1994).

4. Young, J., Berger, R. & Breese, J. Accelerated curing of compacted calcium silicate mortars on exposure to CO_2. *J. Am. Ceram. Soc.* **57**, 394–397 (1974).

5. Rostami, V., Shao, Y., Boyd, A. & He, Z. Microstructure of cement paste subject to early carbonation curing. *Cement and Concrete Research* **42**, 186 (2012).

6. Reuter, D., Gerth, G. & Kirschner, J. *Surface Diffusion*, vol. 360, 489 (Plenum Press, 1997).

7. Ferralis, N., El Gabaly, F., Schmid, A., Maboudian, R. & Carraro, C. Real-time observation of reactive spreading of gold on silicon. *Phys. Rev. Lett.* **103**, 256102 (2009).

8. Rasband, W. ImageJ. http://imagej.nih.gov/ij/ (1997-2013).

9. Schneider, C., Rasband, W. & Eliceiri, K. NIH image to ImageJ: 25 years of image analysis. *Nature Methods* **9**, 671–675 (2012).

10. Juenger, M., Monteiro, P., Gartner, E. & Denbeaux, G. A soft x-ray microscope investigation into the effects of calcium chloride on tricalcium silicate hydration. *Cement and Concrete Research* **35**, 19–25 (2005).

11. Bullard, J. *et al.* Mechanisms of cement hydration. *Cement and Concrete Research* **41**, 1208–1223 (2011).

12. Thomas, J. *et al.* Modeling and simulation of cement hydration kinetics and microstructure development. *Cement and Concrete Research* **41**, 1257–1278 (2011).

13. Haselbach, L. Potential for carbon dioxide absorption in concrete. *Journal of Environmental Engineering* **135**, 465–472 (2009).

14. Black, L. Raman spectroscopy of cementitious materials. *Spectroscopic Properties of Inorganic and Organometallic Compounds: Materials and Applications* **40**, 72–127 (2009).

15. Kirkpatrick, R., Yarger, J., McMillan, P., Ping, Y. & Cong, X. Raman spectroscopy of CSH, tobermorite, and jennite. *Advanced Cement Based Materials* **5**, 93–99 (1997).

16. Padanyi, Z. The Raman spectrum of $Ca(OH)_2$. *Solid State Communications* **8**, 541–543 (1970).

17. Martínez-Ramírez, S. & Fernández-Carrasco, L. *Raman spectroscopy: application to cementitious systems* (Nova Science Publishers, 2011).

18. Potgieter-Vermaak, S., Potgieter, J. & Van Grieken, R. The application of Raman spectrometry to investigate and characterize cement, part I: A review. *Cement and concrete research* **36**, 656–662 (2006).

19. Downs, R. The RRUFF project: an integrated study of the chemistry, crystallography, raman and infrared spectroscopy of minerals. *9th General Meeting of the International Mineralogical Association* **O03-13** (2006). URL `http://rruff.info/`.